Journal of Sound and Vibration (1995) **188**(1), 39–54

SNORING: LINEAR STABILITY ANALYSIS AND *IN-VITRO* EXPERIMENTS

Y. Aurégan and C. Depollier

Laboratoire d'Acoustique de l'Université du Maine, U.R.A. C.N.R.S. 1101, *Av. O. Messiaen, B.P.* 535, 72017 *Le Mans Cedex, France*

(*Received* 27 *September* 1993, *and in final form* 24 *October* 1994)

A theoretical and experimental study is presented of the aeroelastic instability of the human soft palate, which can explain the occurrence of snoring. The soft palate is modelled by a beam clamped at its leading edge and free at its trailing edge. The continuous and discrete cases are investigated. Only the two first modes of vibration of the soft palate are taken into account. The flow is incompressible, inviscid and one-dimensional. Structural damping and flow nonstationarities can be considered. Theory shows that the soft palate loses its stability by flutter and that this instability is mainly controlled by a single dimensionless parameter which can be easily interpreted from a medical point of view. An experimental apparatus which produces sounds very close to human snoring is described. Agreement between theory and experiments is good.

1. INTRODUCTION

Flow-induced vibrations are very common phenomena which take place in various situations: e.g., the flutter of a flag in the wind or the musical sound produced by a reed instrument. In any case, this phenomenon can be seen to be a result of the loss of stability of a mechanical oscillator interacting with a continuous flow.

The linear theory applied to such systems shows that the amplitude of the oscillations grows exponentially when the instability occurs: i.e., when a control parameter, for example the flow velocity, reaches a critical value. For the model to remain valid following the onset of instability, non-linear terms have to be inserted in the equation of motion. Therefore, the dynamical behaviour of these physical systems is governed by essentially non-linear equations of motion. However, when one studies the stability of the system the equations of motion can be linearized about equilibrium, and hence one considers the onset of oscillations. In this case, for a subsonic flow, the simplest modeling of an oscillatory bifurcation implies two degrees of freedom which characterize the essential properties of the systems. These allow one to distinguish two classes of systems: first, systems for which the two degrees of freedom involve one mechanical oscillator and one flow oscillation respectively, and second, systems involving two mechanical oscillators coupled by the fluid flow. Among the most typical systems the reed instruments and the aeolian harp [1] belong to the first class, while the vocal cords [2], elastic pipes conveying an incompressible fluid [3], or panels in uniform flow [4] belong to the second one. Human snoring is produced by a system which also belongs to the second class. Medical observations show that this phenomenon is due to the soft palate vibrations induced by the inspiratory flow [5]. Roughly, it can be understood as follows: in some cases the soft palate becomes aeroelastically unstable and when it bumps against the pharingeal walls, it closes the upper airways, causing large changes of pressure in the inspiratory airflow and producing its

0022–460X/95/460039 + 16 $12.00/0

characteristic noise. Recently, snoring has received a great deal of attention from a medical point of view because of its relationships with the sleep apnea syndrome.† These studies are mainly devoted to the effects of snoring on health, to the treatment effects [6] or to the description of the noise produced [7, 8]. To our knowledge, little attention has been given to the biomedical source of snoring except for the work of Gavriely and Jensen [9] which presents a model explaining the closing of the upper airways during snoring but not the reopening. Thus the aim of this paper is to answer as simply as possible the following questions: *Why does one snore? What are the conditions required for snoring?*

In order to find a biomechanical model providing answers to these questions, two main points of view can be found in the literature. In the first, the length of the flexible structures under consideration is infinite or at least much greater than the wavelength of the elastic perturbation wave in the structure. Therefore the main structure characteristics can be seen as a wave speed and the stability criterion does not involve boundary conditions in the wave propagation direction [10]. In the second, the size of the vibrating structure is of the order of the perturbation wavelength (small aspect ratio). In this case, the simplest way to take the boundary conditions into account is a modal expansion in combination with Galerkin's method. In the snoring phenomenon, the length of the soft palate (~ 4 cm) is of the same order of magnitude as the typical wavelength for transverse vibrations.‡ From the above considerations this means that modal expansion will make our study easier, and the simplest modelling will be a two-mode flutter.

2. MODEL DESCRIPTION

The soft palate is a very flexible structure located at the confluence of the nasal and buccal tracks where they connect with the pharynx, as shown in Fig. 1(a). During snoring, the soft palate vibrates at a frequency of 20–80 Hz. Therefore, its transverse vibrations are far faster than the motion of the surrounding walls (the tongue, and the posterior wall of the pharynx have typical oscillation times of the order of 1 or 2 seconds). As a result, during snoring the structural behaviour of the upper airways can be modelled as one of a flexible structure in a rigid walled channel (see Figure 1(b)).

For simplicity, we consider a two-dimensional situation and in this case, relative to the equilibrium state, the motion of the structure is a solution of the equation

$$\mathscr{L}_{x,t}[w(x, t)] = \Delta P(x, t), \tag{1}$$

where $\Delta P(x, t)$ is the pressure difference, produced by the motion, between the two sides of the plate, $w(x, t)$ is the transverse displacement of the plate from the equilibrium position, and $\mathscr{L}_{x,t}[\ \cdot\ ]$ is a second order in time linear differential operator (with the co-ordinates x and t) which will be specified by physical modelling further on. For example, in the case of a continuous rectangular beam, this operator is

$$\mathscr{L}_{x,t}[w(x, t)] = (Ee^3/12)\ \partial^4 w(x, t)/\partial x^4 + \mu e\ \partial^2 w(x, t)/\partial t^2,$$

†A sleep apnea is a respiratory pause (during more than ten seconds) caused by the collapse of the soft parts of the upper airways during breathing.

‡The wavelength (λ) used as a characteristic length is defined from the transverse vibrations of prismatic beam theory by the relation:

$$\lambda = \{Ee^2/12\varrho\omega^2\}^{1/4}.$$

where E is the Young's modulus, e is the thickness of the beam, ϱ is the mass density, and ω is the angular frequency. In snoring their estimated values are as follows: $E \sim 10^6 \mathrm{N\,m^{-2}}$; $e \sim 5 \times 10^{-3}$m; $\varrho \sim 10^3 \mathrm{kg\,m^{-3}}$; $\omega \sim 125 \mathrm{rad\,s^{-1}}$.

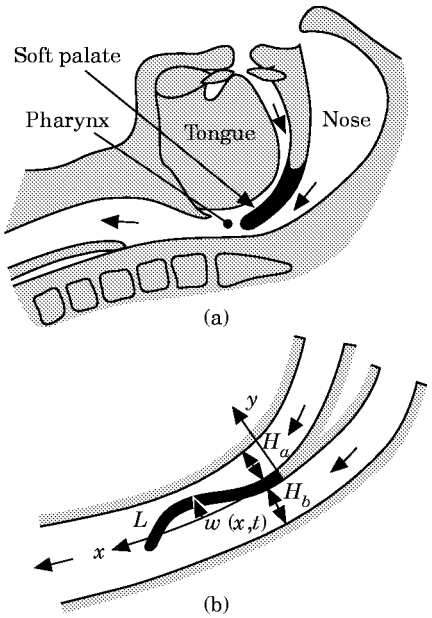

Figure 1. (a) A schematic description of the human pharynx; (b) a model of the pharynx (the moving part is in black).

where E, e and μ are, respectively, the Young's modulus, the thickness and the density of the beam.

2.1. MODAL EXPANSION METHOD

For the solution of equation (1), $w(x, t)$, in the form of an infinite expansion in terms of dimensionless spatial natural modes $\psi_m(x)$, one can write

$$w(x, t) = \sum_{i=1}^{\infty} A_i(t)\psi_i(x), \tag{2}$$

where the functions ψ_m satisfy the same boundary conditions as $w(x, t)$,

$$w(0, t) = 0, \qquad \partial w(x, t)/\partial x|_{x=0} = 0, \qquad \partial^2 w(x, t)/\partial x^2|_{x=L} = 0, \qquad \partial^3 w(x, t)/\partial x^3|_{x=L} = 0,$$

and are the eigenfunctions of the spatial part $\mathscr{L}_x[\ \cdot\ ]$ of the operator $\mathscr{L}_{x,t}[\ \cdot\ ]$.

For compatible geometries and simple enough boundary conditions, one can determine analytical expressions for the eigenmodes $\psi_m(x)$. For example, in the case of a flat plate clamped at one end and free at the other, the eigenmodes form a set of orthogonal functions if one neglects dissipation in the structure [11]. For more complicated geometries, one can still find, by numerical methods, a set of functions which approximately satisfies the orthogonality condition. Using Galerkin's method [12], one changes the partial differential equation (1) into an infinite set of ordinary differential equations for the amplitudes $A_n(t)$:

$$\frac{\mathrm{d}^2 A_n(t)}{\mathrm{d}t^2} + \omega_n^2 A_n(t) = \frac{1}{M_n}\int_0^L \psi_n(x)\, \Delta P(x, t)\, \mathrm{d}x, \qquad n = 1, \ldots, \infty. \tag{3}$$

In this equation, the modal mass per unit width, M_n, is given by $M_n = m_n \mu e L$, where

$$m_n = (1/L)\int_0^L \psi_n^2(x)\,\mathrm{d}x$$

is a dimensionless parameter depending on the modal shape; μ, e and L are, respectively, the density, the thickness and the length of the soft palate and ω_i represents the natural frequencies of equation (1) for $\Delta P \equiv 0$ (free oscillations).

2.2. FLUID MODEL

The aerodynamic pressure difference $\Delta P(x, t)$ is related to the motion of the structure in the fluid, and is the result of various phenomena. In our particular case, the fluid flows in a narrow channel, between the wall and the moving structure, and so the streamline curvature effects which are very important in free field conditions [4] can be neglected. We assume a quasi-parallel flow and as a consequence a uniform pressure across the flow. Typically, the maximal inspiratory flow rate is about $1\,\mathrm{l\,s^{-1}}$ and the cross-section of the channel about $2\,\mathrm{cm^2}$, so that a typical velocity of the fluid is $5\,\mathrm{m\,s^{-1}}$. This leads to a maximal Reynolds number of 3000. The pressure drop induced by friction losses along the soft palate is therefore negligible in comparison to the inertial effects as long as the height of the channel is more than 1 mm [13]. These friction effects are useful only in the explanation of snoring sound production to avoid a singular flow behaviour upon closing of the channel. Here, in the description of the onset of snoring, they are negligible. For reasons of simplicity, we will further assume a uniform flow when calculating inertial effects in the channels.

The mean steady velocity of the air in both channels is given by the ratio of the upstream pressure drop (in the mouth and in the nose). We will further consider for the sake of simplicity that this ratio is equal to 1 so that the velocity is the same in both channels. However, this model can be simply generalized to other cases (for instance, to the case in which one of the channels is closed). This assumption avoids complex calculations when we take unsteadiness into account.

If we define a Strouhal number by the ratio of the snoring fundamental frequency (about 50 Hz) times the length L of the soft palate over the typical fluid velocity U_0, we find a typical value of 0·4. Therefore, the non-stationary flow effects are essential in snoring. Because the system is small compared to the acoustical wavelength corresponding to f_0 and as the Mach number is small, the flow is locally incompressible.

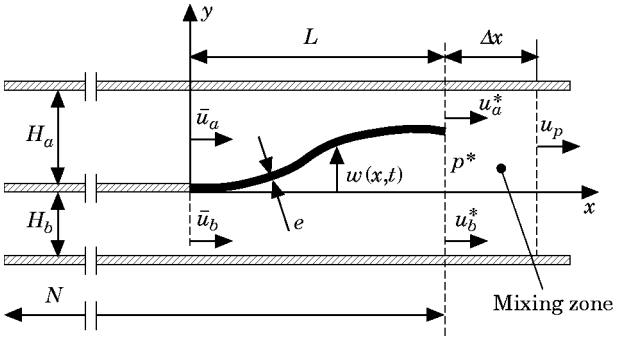

Figure 2. A description of some notations used in the model.

2.3. BASIC EQUATIONS

The following equations are being formulated for the upper (a) channel and similar equations with $w(x, t)$ replaced by $-w(x, t)$ hold for the lower (b) channel, with now the subscript b instead of a.

The first equation expresses the conservation of mass, and upon assuming that the fluid is incompressible, it can be written in the form (for the notation, see Figure 2):

$$(\partial/\partial t)\{H_a - w(x, t)\} + (\partial/\partial x)\{u_a(x, t)(H_a - w(x, t))\} = 0. \tag{4}$$

The fluid velocity can be split into a steady flow velocity U_a and a fluctuating part $\tilde{u}_a(x, t)$: $u_a(x, t) = U_a + \tilde{u}_a(x, t)$. Using this definition and equation (4), one obtains

$$\tilde{u}_a(x, t) = \frac{\partial W(x, t)/\partial t + U_a w(x, t) + H_a \bar{u}_a}{H_a - w(x, t)}, \tag{5}$$

where the potential integral of the displacement $w(x, t)$ is

$$W(x, t) = \int_0^x w(x', t)\, \mathrm{d}x'$$

and $\bar{u}_a = \tilde{u}_a(0, t)$. One can linearize equation (5) by expanding $\tilde{u}_a(x, t)$ in a power series in the small parameter $w(x, t)/H_a$. The zero-order term is related to the equilibrium condition and, upon keeping only the first order term, the solution of equation (4) can be written as

$$\tilde{u}_a(x, t) = \bar{u}_a + (1/H_a)\{\partial W(x, t)/\partial t + U_a w(x, t)\}. \tag{6}$$

The pressure is determined accordingly by the unsteady Bernoulli equation:

$$p_a(x, t) - p_a(0, t) = \frac{\varrho}{2}\{(U_a + \bar{u}_a)^2 - (U_a + \tilde{u}_a(x, t))^2\} - \varrho \int_0^x \frac{\partial \tilde{u}_a(x', t)}{\partial t}\, \mathrm{d}x'. \tag{7}$$

Like the velocity, the pressure is split into a steady part P_a and a fluctuating part $\tilde{p}_a$, i.e., $p_a(x, t) = P_a(x) + \tilde{p}_a(x, t)$, while the input pressure is written as $p_a(0, t) = P_a(0) + \bar{p}_a(t)$. To first order, equation (7) becomes

$$\tilde{p}_a(x, t) = \bar{p}_a(t) = \frac{\varrho}{H_a}\left\{U_a^2 w(x, t) + 2U_a \frac{\partial W(x, t)}{\partial t} + \frac{\partial^2 \mathscr{W}(x, t)}{\partial t^2}\right\} - \varrho x \frac{\mathrm{d}\bar{u}_a(t)}{\mathrm{d}t}, \tag{8}$$

where

$$\mathscr{W}(x, t) = \int_0^x W(x', t)\, \mathrm{d}x'.$$

To determine the pressure completely, one must take into account the following (the superscripted asterisk notation here means the value of the function at $x = L$): the equality of the pressure at the end ($x = L$) of the channels,

$$p_a(L, t) = p_b(L, t) = p^*(t); \tag{9}$$

the input impedance equations,

$$\bar{p}_a(t) = -Z_a \bar{u}_a(t), \qquad \bar{p}_b(t) = -Z_b \bar{u}_b(t); \tag{10}$$

the conservation of mass and of momentum in the mixing zone of length ΔX (see Figure 2),

$$H_a u_a^* + H_b u_b^* = H_p \tilde{u}_p, \qquad p^* = \tilde{p}_p + \varrho\, \Delta X\, \partial \tilde{u}_p / \partial t, \tag{11}$$

where $H_p = H_a + H_b + e$, $\tilde{u}_p$ and $\tilde{p}_p$ are the fluctuating parts of the velocity and of the pressure downstream of the mixing zone; the output impedance equation:

$$\tilde{p}_p(t) = Z_p \tilde{u}_p(t). \tag{12}$$

The equations (6) and (8) for the channels a and b, and (9)–(12) allow the calculation of the pressure p_a and p_b.

For simplicity, we consider, in section 2.4, a quasi-stationary model without viscous losses. It leads to a flutter bifurcation with a very simple instability condition. We shall consider, in the later section, the effects of the unsteadiness and of the upstream viscous losses on this condition.

2.4. QUASI-STATIONARY FRICTIONLESS MODEL

In snoring, as in our experimental system, the Strouhal number fL/U is of the order of 0·1. Then, in a first approximation, we consider a quasi-stationary model and the time derivatives of the flow parameters drop out. Furthermore, if we consider that the viscous losses upstream of the soft palate are the same in both channels, Bernoulli's theorem with the equality of pressure at the end of the soft palate (9) implies that the steady air velocity is the same in both channels: $U_a = U_b = U$. With those assumptions, the pressure difference between both sides of the soft palate reduces to

$$\Delta P(x, t) = \varrho \{(1/H_a) + (1/H_b)\} U^2 (w(x, t) - w^*(t)), \tag{13}$$

where $w^*(t) = w(L, t)$. In the following, we write $1/H = (1/H_a) + (1/H_b)$. Upon introducing the dimensionless time $\tau = \omega_1 t$ and length $\xi = x/L$, equation (3) becomes

$$\frac{\mathrm{d}^2 a_n(\tau)}{\mathrm{d}\tau^2} + \beta_n^2 a_n(\tau) = -\frac{\varrho U^2}{\omega_1^2 \mu e H} \left\{ \frac{\alpha_n \psi_n^* - 1}{m_n} a_n(\tau) + \sum_{\substack{j=1 \\ j \neq n}}^{\infty} \frac{\alpha_n \psi_j^*}{m_n} a_j(\tau) \right\}, \tag{14}$$

where $a_n(\tau)$ is the dimensionless A_n/L, $\beta_n = \omega_n/\omega_1$, ψ_n^* is the value of ψ_n when $\xi = 1$ and

$$\alpha_n = \int_0^1 \psi_n(\xi)\, \mathrm{d}\xi.$$

Note that β_n and the term in brackets on the right side of equation (14) depend only on the modal shapes. All the other physical parameters, which are involved in the stability analysis, can be reduced to a single dimensionless control parameter, $\gamma = \varrho U/\omega_1^2 \mu e H$, which characterizes the ratio of inertial forces in the fluid to stiffness forces of the soft palate.

If the viscous losses are not the same in both channels (for instance, if one channel is closed) this parameter can be more generally written as $\gamma = (\varrho/\omega_1^2 \mu e)\{(U_a^2/H_a) + (U_b^2/H_b)\}$. In the specific case of a two mode model, equation (14) can be written as

$$\mathrm{d}x/\mathrm{d}\tau = \mathbf{A}_\gamma \mathbf{x}, \tag{15}$$

where

$$\mathbf{A}_\gamma = \begin{bmatrix} \mathbf{0} & \mathbf{I} \\ -\mathbf{K}_\gamma & \mathbf{0} \end{bmatrix}, \qquad \mathbf{x} = \begin{pmatrix} x_1 \\ x_2 \\ x_3 \\ x_4 \end{pmatrix},$$

$$\mathbf{K}_\gamma = \begin{bmatrix} 1+\gamma a_{11} & \gamma a_{12} \\ \gamma a_{21} & \beta_2^2+\gamma a_{22} \end{bmatrix}$$

is the stiffness matrix, $x_1 = a_1(\tau)$, $x_2 = a_2(\tau)$, $x_3 = \mathrm{d}a_1(\tau)/\mathrm{d}\tau$, $x_4 = \mathrm{d}a_2(\tau)/\mathrm{d}\tau$, and $a_{ij} = (\alpha_i \psi_j^* - \delta_{ij})/m_i$. (The numerical values of β_2 and a_{ij} are given in the appendix for the two particular cases of a clamped–free uniform beam and a bi-articulated beam.)

To investigate the stability of the equilibrium, we assume an exponential form for the vector $\mathbf{x} = \xi\, \mathrm{e}^{s\tau}$. The stability is then determined by the real part of the eigenvalues s_i, $i = 1, \ldots, 4$, given by a quadratic equation

$$\det(\mathbf{A}_\gamma - s_i \mathbf{I}) = s_i^4 + \mathrm{tr}(\mathbf{K}_\gamma) s_i^2 + \det(\mathbf{K}_\gamma) = 0. \tag{16}$$

The system (15) is generically stable as long as the conditions

$$\mathrm{dis}(\mathbf{K}_\gamma) = \mathrm{tr}^3(\mathbf{K}_\gamma) - 4\det(\mathbf{K}_\gamma) > 0, \qquad \det(\mathbf{K}_\gamma) > 0 \qquad \text{and} \qquad \mathrm{tr}(\mathbf{K}_\gamma) > 0$$

are valid. The eigenvalues are then purely imaginary numbers, two by two conjugated ($s_1 = -s_3$, $s_2 = -s_4$). The instability arises when at least one eigenvalue (e.g., s_1) has a real part becoming positive. This can occur in two ways: (i) when $\mathrm{tr}(\mathbf{K}_\gamma)$ or $\det(\mathbf{K}_\gamma)$ becomes negative; in this case, $\mathrm{Im}(s_1) = 0$; this instability is called *divergence*; (ii) when $\mathrm{dis}(\mathbf{K}_\gamma)$ becomes negative; in this case, the two pairs of conjugated eigenvalues coincide ($s_1 = s_2 = -s_3 = -s_4$) before $\mathrm{Re}(s_1) > 0$; this instability is called *flutter*.

In the case of a beam clamped at one end and free at the other, the aerodynamic stiffness coefficient a_{11} is positive. This shows that the stiffness (and therefore the frequency) of the first mode increases when γ increases (i.e., when the flow velocity increases, when the heights H_a and/or H_b decreases, etc.). On the other hand, the stiffness of the second mode decreases with γ ($a_{22} < 0$) because of the modal shape. The coupling aerodynamic coefficients a_{12} and a_{21} are opposite in sign, showing that the coupling, through the boundary conditions at $x = L$, is non-conservative [14]. For this kind of system, when γ is increased the first instability encountered is the flutter instability ($\mathrm{dis}(\mathbf{K}_\gamma) = 0$ while $\mathrm{tr}(\mathbf{K}_\gamma) > 0$ and $\det(\mathbf{K}_\gamma) > 0$). So the critical value of the control parameter γ is

$$\gamma_{cr} = (\beta_2^2 - 1)/(a_{11} - a_{22} + 2\sqrt{-a_{12}a_{21}}). \tag{17}$$

From the numerical values given in the Appendix, the critical value of γ is 8·05 for a clamped–free uniform beam and 2·43 for a bi-articulated beam. The difference between these values comes mainly from the difference in β_2 (ratio of the second on the first natural frequency) for the two beams under consideration.

2.5. INFLUENCE OF DAMPING

The destabilizing effect of damping forces in a non-conservative flutter-type system has been known for a long time [15]. The non-genericity of the undamped system [16] constrains us to take the damping into account, however weak it is. Two main kinds of damping happen in the system under consideration: structural damping, which acts on the system even without flow; flow-induced damping, which results from the flow nonstationarities.

The dimensionless structural damping matrix can be written:

$$\epsilon\mathbf{C}=\epsilon\begin{bmatrix} c_{11} & c_{12} \\ c_{21} & c_{22} \end{bmatrix},$$

where c_{11}, c_{12}, c_{21} and c_{22} are dimensionless coefficients depending on the damping modeling and on the modal shapes (their numerical values are given in the Appendix), ϵ is a dimensionless number involving the damping value, the modal mass and the first natural frequency. If one considers only this damping in the system, equation (15) can be written as

$$\frac{\mathrm{d}\mathbf{x}}{\mathrm{d}\tau}=\begin{bmatrix} \mathbf{0} & \mathbf{I} \\ -\mathbf{K}_\gamma & -\epsilon\mathbf{C} \end{bmatrix}\mathbf{x}. \tag{18}$$

In this case, as long as the damping is small with respect to the critical damping, the value of ϵ has no influence on the values of γ for which the instability occurs. This value can be found by solving the equations [17]

$$\Omega_d^4=\mathrm{tr}\,(\mathbf{K}_\gamma)\Omega_d^2+\det\,(\mathbf{K}_{\gamma_d})=0, \tag{19}$$

$$\mathrm{tr}\,(\mathbf{C})\Omega_d^2=\beta_2^2 c_{11}+c_{22}+\gamma_d(a_{11}c_{22}+a_{22}c_{11}-a_{12}c_{21}-a_{21}c_{12}), \tag{20}$$

where Ω_d is the imaginary part of the eigenvalue of equation (18) (becoming unstable, $\mathrm{Re}\,(s_1)=0$) and γ_d is the critical control parameter with structural damping.

The solid line in Figure 3, for a clamped–free uniform beam, shows Ω_d^2 *vs.* γ resulting from equation (19), which is the same as equation (16) when s_i is purely imaginary, and equation (20). In this case, the bifurcation takes place on the first mode (point D) for a value of γ lower than the undamped case (point A).

During its motion, the beam produces pressure changes in the fluid, not only proportional to the displacement, as we have seen, but also proportional to the velocity and to the acceleration: the flow-induced damping and the added mass. To introduce those second order phenomena, we must take into account the non-stationarity of the flow. For that, we use the complete set of fluid equations given in section 2.3. For simplicity, we

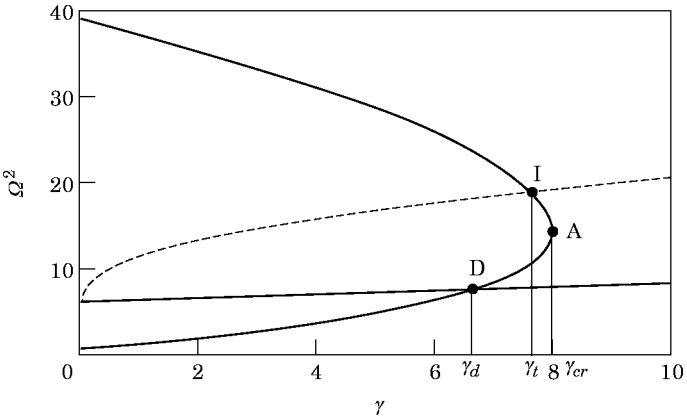

Figure 3. Graphical solutions of equations (19) and (20) for a continuous beam with structural damping (——) and for a continuous beam with structural and flow-added damping (– – – –).

assume that the a and b channels (upstream of the soft palate) are rigid open pipes of length $N-L$ (in the low frequency approximation). Therefore, equations (10) become

$$\bar{p}_a(t) = -\varrho(N-L)\,\mathrm{d}\bar{u}_a(t)/\mathrm{d}t, \qquad \bar{p}_b(t) = -\varrho(N-L)\,\mathrm{d}\bar{u}_b(t)/\mathrm{d}t. \tag{21}$$

With these assumptions, equation (9) is written

$$p^*(t) = -\varrho\left(N\frac{\mathrm{d}\bar{u}_a(t)}{\mathrm{d}t} + \frac{A^*(t)}{H_a}\right) = -\varrho\left(N\frac{\mathrm{d}\bar{u}_b(t)}{\mathrm{d}t} - \frac{A^*(t)}{H_b}\right), \tag{22}$$

where

$$A^*(t) = U^2 w(L, t) + 2U(\partial/\partial t)W(L, t) + (\partial^2/\partial t^2)\mathscr{W}(L, t).$$

In this case, the non-stationary flow "turns" around the soft palate, so the output impedance Z_p and the added length ΔX do not play any part in the problem. The pressure difference between both sides is

$$\Delta P(x, \tau) = \frac{\varrho}{H}\left\{U^2(w - w^*) + 2U\omega_1\frac{\partial}{\partial\tau}(W - W^*) + \omega_1^2\frac{\partial}{\partial\tau^2}(\mathscr{W} - \mathscr{W}^*)\right.$$

$$\left. + \frac{L-x}{N}\left[U^2 w^* + 2U\omega_1\frac{\partial W^*}{\partial\tau} + \omega_1^2\frac{\partial^2\mathscr{W}^*}{\partial\tau^2}\right]\right\}, \tag{23}$$

where the asterisk indicates the value of the function when $x = L$. The first term in brackets is the quasi-stationary stiffness term of equation (13) in section 2.4. The second term is due to flow-induced damping and the third to added mass. The last term represents the influence of the upstream rigid pipes on the pressure. It also involves added stiffness, damping and mass. Unlike in water flow, the added mass has little influence in air flow problems at low frequency. Therefore it is not taken into account here. The length L of the soft palate is weaker than the length $N-L$ of the upstream pipes, so their influence vanishes in comparison with the local contribution. With all these simplifications, the nonstationarity acts only on the damping matrix which becomes $\epsilon\mathbf{C} + \gamma\mathscr{S}_t\mathbf{D}$, where $\mathscr{S}_t$ is the Strouhal number ($\omega_1 L/U$) and the components of $\mathbf{D}$ depend on the modal shape (their numerical values are given in the Appendix). The Strouhal number can also be written as $\mathscr{S}_t = \sqrt{(\varrho/\mu)(L^2/eH)}(1/\sqrt{\gamma})$, where the first square root is typically of the order of unity. Adding the flow-induced damping to equation (20) when $\epsilon = 0{\cdot}1$ and $\mathscr{S}_t = 0{\cdot}5/\sqrt{\gamma}$ leads to the broken line curve in Figure 3. Bifurcation takes place on the second mode (point I) for a value of γ close to the value without damping.

3. EXPERIMENTS

In order to test the results of the stability analysis, experiments were performed with the system shown in Figure 4. In this apparatus, the vibrating part is either a flexible rectangular beam (made of elastomer) or a beam formed by two rigid bodies linked by a plastic film. The mechanical characteristics of the beams are given in Table 1. In both cases a piezo-electric film is inserted in the beam near the fixation point to have an indication of the beam motion. The beam is located between two adjustable walls which allow variation of the channel heights H_a and H_b. Air is extracted from a large reservoir ($\sim 0{\cdot}5\ \mathrm{m}^3$), which represents the lungs, by a vacuum pump. The apparatus is shaken to ensure measurable motions of the beam even without flow. The input signal to the shaker

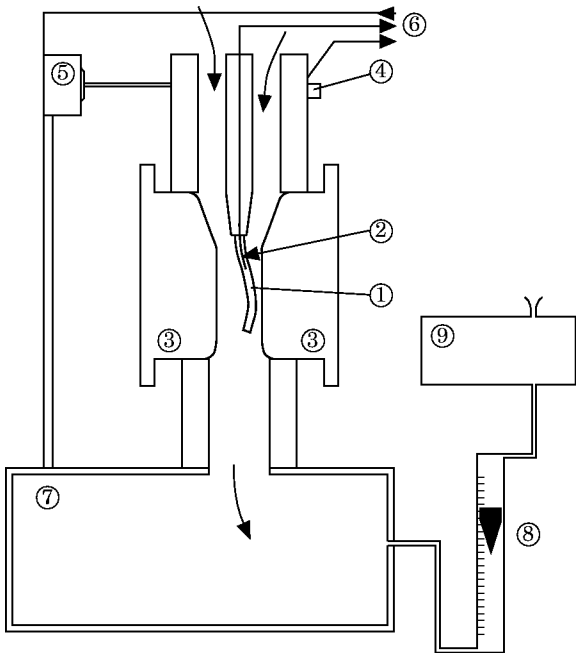

Figure 4. The experimental apparatus. 1, Flexible beam; 2, piezo-electric film (SOLEF 40 μm, Solvay & Co); 3, adjustable walls; 4, accelerometer (B & K 4575); 5, shaker (B & K 4810); 6, to/from the FFT analyzer (HP 3562A); 7, reservoir; 8, flow meter; 9, vacuum pump (L 250 DD, PIAB).

is a broadband noise. The apparatus motion is considered as the excitation and the piezo-electric film signal as the response. This makes possible the measurement of the transfer function with and without flow. However, this notion of transfer function no longer has the same meaning when part of the excitation comes from turbulent pressure fluctuation in the flow. The transfer function without flow allows the calculation of the Young's modulus and of the structural damping in the elastomer beam and the calculation of the articulation stiffness and of the structural damping in the bi-articulated beam.

When one increases the flow velocity very slowly, the frequency of the first resonance increases while the damping (which is given by the bandwidth at -3 dB) also increases (see Figure 5). In contrast, the frequency of the second resonance decreases and the transfer function displays a sharper and sharper peak until the instability takes place. When both channels are open, the instability occurs very abruptly: just before, the amplitude of the motion is weak, and just after, the beam hits at least one of the walls.

One can notice, in Figure 5, that there is a shift in the air velocity between those of the theory and the experimental results. This is the result of the clearance on the transverse sides of the beam required for working without friction. To take it into account, one must use a ratio of the effective width to the real width of $\sim 90\%$ in the control parameter γ.

In Figure 6 is shown the critical velocity as a function of the equivalent height $H=(H_a^{-1}+H_b^{-1})^{-1}$ in the case of the bi-articulated beam with both channels open. Theory and experiments are in good agreement except when H_a and H_b are very different. This disagreement results from the neglected viscous losses, which imply a difference in the air velocities between the two channels, as explained in section 2.2. In Figure 7, the same kind of results are shown when one of the channels is closed. In this case, the instability is more difficult to define because the growth of the amplitude of the motion is more gradual than in the previous case. This can be explained by the flow separation along the beam, which is not compensated by the pressure distribution on the other side of the beam where there

TABLE 1

Mechanical characteristics of the beams used in the experimental apparatus

	Length, L (mm)	Thickness e (mm)	Width (mm)	Density (kg m^{-3})	Young's modulus (N m^{-2})	Dimensionless damping
Bi-articulated beam	26 (each)	4·2	43	1170		0·16
Elastomer beam	62, 56, 44, 40	2·7	43	1246	$1{\cdot}8 \times 10^6$	0·1

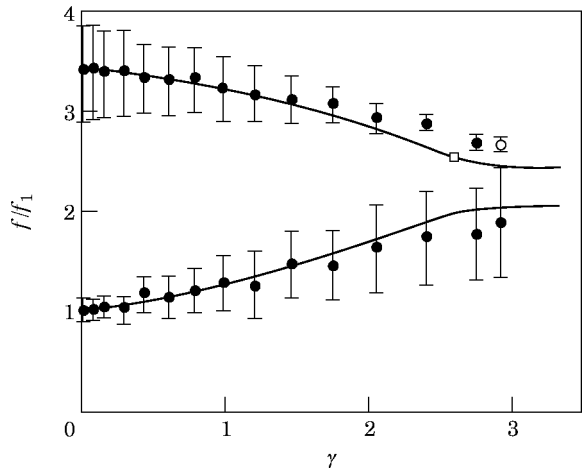

Figure 5. The dimensionless frequency *vs*. the control parameter γ for the bi-articulated beam when $H_a = H_b = 10{\cdot}2$ mm. ——, Theory; ●, experimental frequency; |——|, experimental bandwidth at -3 dB; □, theoretical bifurcation point; ○, experimental bifurcation point.

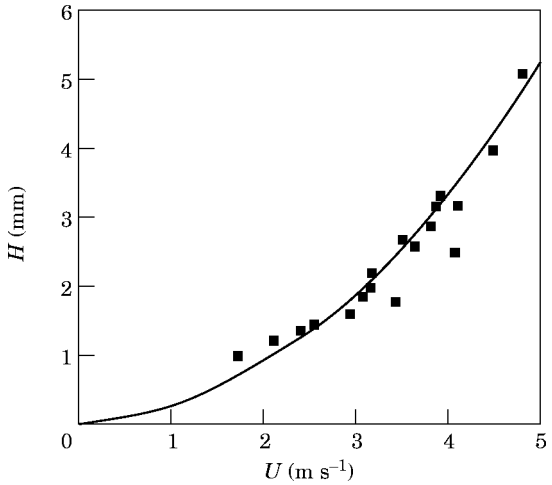

Figure 6. The equivalent height of the channels (H_a and H_b range from 2 to 20 mm) *vs*. the critical velocity when both channels are open (bi-articulated beam). ——, Theory taking into account the effective width; ■, experiments.

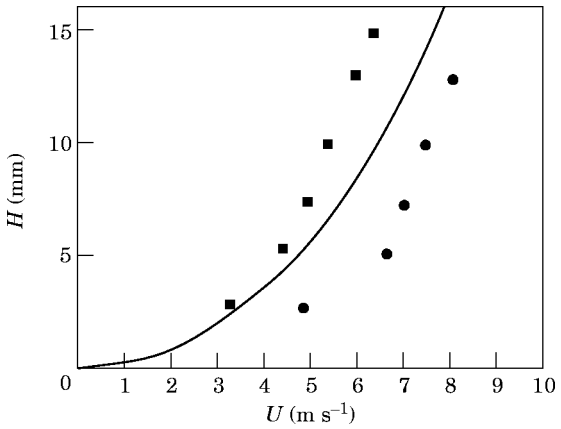

Figure 7. As Figure 6, but with one channel closed.

is no flow. Therefore, we show two points: when the amplitude of the motion becomes twice the amplitude without flow (square dots) and when the beam begins to bump the wall (circle dots). One can see in Figure 8 that the critical velocity is inversely proportional to the square of the length of the elastomer beam as predicted by the theory (ω_1 inversely proportional to L^2).

Thus the linear theory predicts the value of the velocity U_i at which the instability of a beam between two walls occurs when one progressively increases the flow. However, the bifurcation occurs for velocities lower than U_i for an impulsive start of the flow. In the same way, when one progressively decreases the flow, the apparatus returns to stability for a value of velocity U_r lower than U_i (see Figure 9). Between these two values, the system has, for one velocity, two limit cycles: the equilibrium point and the motion hitting the walls. The asymptotic behaviour of the system depends on initial conditions: small perturbations lead to the equilibrium while large perturbations (for instance, the starting vortex in an impulsive start of the flow) lead to the other limit cycle.

After the instability, the free end of the beam bumps into the walls. The frequency of this motion is slightly greater than the frequency of the second mode just before bifurcation (see Figure 9). At this stage, the level of the sound produced is low. When one still increases the velocity ($U > U_{2C}$), the contact between the beam and the walls takes place not only

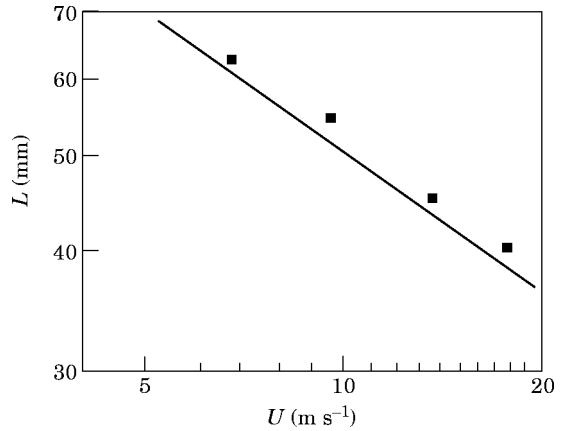

Figure 8. A log–log plot of the length of the flexible beam *vs*. the critical velocity when both channels are open ($H_a = 3{\cdot}5$ mm, $H_b = 5$ mm). ——, Theory taking into account the effective width; ■, experiments.

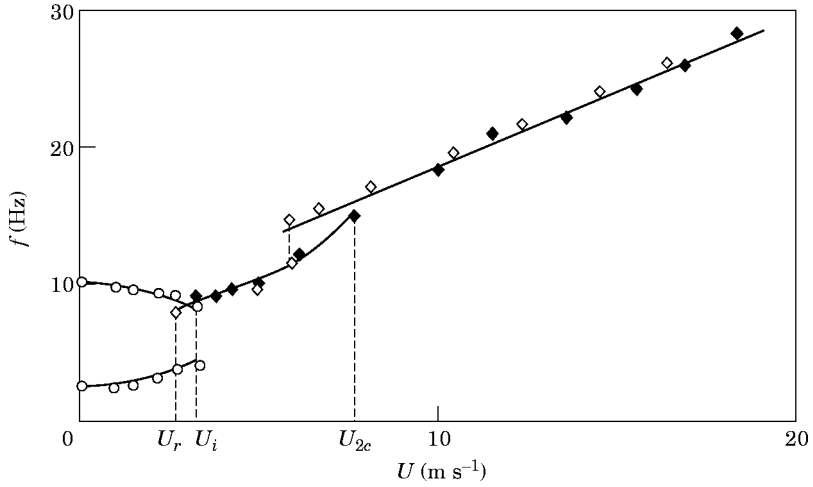

Figure 9. The mean frequency of the motion of the bi-articulated beam *vs*. mean velocity ($H_a = 3$ mm, $H_b = 5$ mm). ○, Stable weak motion; ◆, unstable motion increasing velocity; ◇, unstable motion decreasing velocity.

at the free end but also along the mid-part of the beam and the apparatus produces a loud sound very similar to natural snoring (see Figure 10). The transition between those two behaviours also has hysteresis. For the two-contacts motion, flow visualizations and hot wire velocity measurements show that the flow becomes complex (dynamical flow separation, vortex formation, etc.). Despite this, the fundamental frequency of the motion increases almost linearly with the air velocity (see Figure 9).

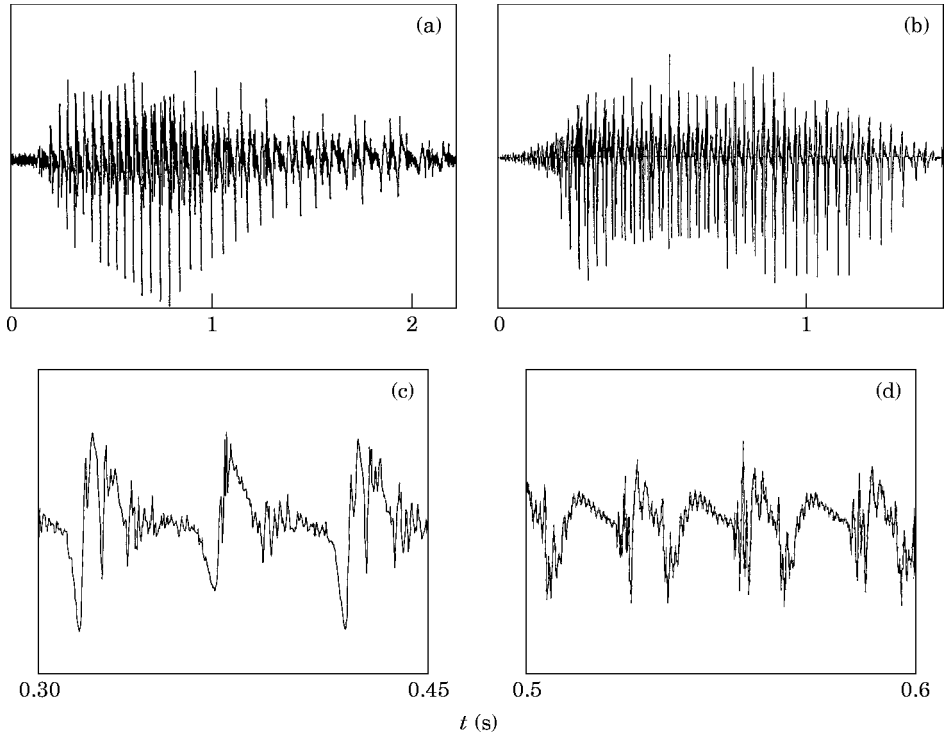

Figure 10. Sound signals of the experimental apparatus (a), (b) and of a simulated snore (c), (d).

4. CONCLUSIONS

A quasi-stationary frictionless model of the oropharynx shows that the instability which leads to snoring is of flutter type. It takes place in the most flexible part of the upper airways tract: i.e., the soft palate. The Bernoulli effect is the most important fluid phenomenon in the description of snoring because, during inspiration, the air flows in a small channel between the posterior pharingeal wall or the tongue and the soft palate. The pressure variations induced by the motion act on both sides of the soft palate (even when the mouth is closed) with a zero pressure difference condition at its free end.

From a mechanical point of view, only a few degrees of freedom are needed in the model because the length of the vibrating structure is of the same order as the transverse vibrations wavelength. Two is the minimal number of degrees of freedom needed. Only one degree cannot model the geometrical changes during one cycle necessary for the soft palate to be able to take out energy from the main flow. More than two degrees leads to more complex calculations for a very weak change in the quantitative results ($\sim 2\%$).

When damping is added to the model (structural and flow added damping), the bifurcation takes place on the second mode for parameter values close to those without damping.

Therefore, the instability is mainly controlled by a single dimensionless parameter: $\gamma = (\varrho U^2/H)(1/\omega_1^2 \mu e)$. This parameter can be split into two parts: one is related to the soft palate characteristics ($1/\omega_1^2 \mu e$, where ω_1 is its first natural frequency, μ is its density and e is its thickness); the other is connected to the flow conditions ($\varrho U^2/H$, where ϱ and U are the density and the velocity of the air and H is an effective height of the upper airways track around the soft palate).

From a physiological point of view, this allows one to distinguish two classes of snorers, as follows.

In the first class, often called "pure snorers", the main cause of snoring is the characteristics of the soft palate. The most effective treatment in this case is the surgical one (uvulopalatopharyngoplasty). It results in the reduction of the length of the soft palate which greatly increases the first natural frequency. An alternative method could consist of increasing artificially the soft palate stiffness.

For the snorers of the second class, the soft palate can be normal and snoring comes from the narrowness of the oropharynx. This is the reason why they can be called "apneic snorers". The treatment is the same as that for apnea: a positive pressure is insufflated through a nasal mask in order to eliminate upper airway occlusion.

In clinical practice, this separation is not so clear and in most patients both phenomena are always more or less involved.

The linear analysis of snoring, presented in this paper, can predict only the onset of snoring when the inspiratory flow increases. A strongly non-linear model is needed to explain the complete motion of the soft palate. Such a model could also describe the large and abrupt changes in the pressure resulting from the closing of the pharyngeal channel and leading to the sound production. Experimental results show that a simple relation between the fundamental frequency of snoring and the flow rate could be expected.

ACKNOWLEDGMENTS

The authors wish to thank A. Hirschberg of the Technical University of Eindhoven and J. L. Racineux and N. Meslier of the Sleep Laboratory of the Angers Hospital for helpful discussions.

Yves Aurégan wishes to acknowledge the financial support of the Crédit Lyonnais Foundation.

REFERENCES

1. H. Bouasse 1930 *Instrument à Vent*, *Tome II*. Paris: Librairie Delagrave.
2. K. Ishizaka and M. Matsudaira 1972 *Speech Communications Research Laboratory Monograph N*8, *Santa Barbara*. Fluid mechanical considerations of vocal cord vibration.
3. M. P. Païdoussis and N. T. Issid 1974 *Journal of Sound and Vibration* **33**, 267–294. Dynamic stability of pipes conveying fluid.
4. A. Kornecki, E. H. Dowell and J. O'Brien 1974 *Journal of Sound and Vibration* **47**, 163–178. On the aeroelastic instability of two-dimensional panels in uniform incompressible flow.
5. F. Chabolle 1988 in *Chronic Rhonchopathy* (C. H. Chouard, editor), 15–19. Anatomic mechanism of snoring.
6. F. G. Issa and C. E. Sullivan 1984 *Journal of Applied Physiology* **54**(2), 528–535. Upper airway closing pressure in snorers.
7. Y. Aurégan, C. Depollier, J. L. Racineux and N. Meslier 1990 *Colloque de Physique* **51**, 789–792. Analyse des signaux de ronflement.
8. J. Rogelio Perez-Padilla, E. Slawinski, L. M. Difrancesco, R. R. Feige, J. E. Remmers and W. A. Whitelaw 1993 *American Review of Respiratory Disease* **147**, 635–644. Characteristics of the snoring noise in patients with and without occlusive sleep apnea.
9. N. Gavriely and O. Jensen 1993 *Journal of Applied Physiology* **74**(6), 2828–2837. Theory and measurements of snores.
10. J. B. Grotberg and S. H. Davis 1980 *Journal of Biomechanics* **13**, 219–230. Fluid-dynamic flapping of a collapsible channel: sound generation and flow limitation.
11. S. Timoshenko, D. H. Young and W. Weaver, Jr. 1974 *Vibration Problems in Engineering*. New York: John Wiley.
12. E. H. Dowell 1974 *Aeroelasticity of Plates and Shells*. Leyden, The Netherlands: Noordhoff.
13. Y. Aurégan and N. Meslier 1993 *Comptes Rendus de l'Académie de Sciences*, *Paris* **316**(II), 1529–1534. Modélisation des apnées obstructives du sommeil.
14. D. S. Weaver 1974 *Journal of Sound and Vibration* **36**, 435–437. On the non-conservative nature of "gyroscopic conservative" systems.
15. Y. Rocard 1960 *Dynamique Générale des Vibrations*. Paris: Masson; third edition.
16. P. J. Holmes 1977 *Journal of Sound and Vibration* **53**, 471–503. Bifurcation to divergence and flutter in flow-induced oscillations: a finite dimensional analysis.
17. S. Nemat-Nasser and G. Herrmann 1966 *Zeitschrift für Angewandte Mathematik und Physik* **17**, 305–313. Some general considerations concerning the destabilizing effect in non-conservative systems.

APPENDIX

In the case of a continuous rectangular beam, the differential operator is:

$$\mathscr{L}_{x,t}[w(x,t)] = (Ee^3/12)\,\partial^4 w(x,t)/\partial x^4 + \mu e\,\partial^2 w(x,t)/\partial t^2,$$

where E, e and μ are, respectively, the Young's modulus, the thickness and the density of the beam. With clamped–free boundary conditions, the first natural frequency is $\omega_1 = 3{\cdot}516eE^{1/2}/L^2\mu^{1/2}$ and the ratio of the second on the first natural frequency is $\beta_2 = 6{\cdot}273$. The following numerical values of the matrix coefficients are independent of the physical parameters. They depend only on the modal shape. The numerical values of the dimensionless flow-added stiffness matrix coefficients are $a_{11} = 0{\cdot}566$, $a_{12} = 1{\cdot}566$, $a_{21} = 0{\cdot}868$ and $a_{22} = -1{\cdot}868$. The numerical values of the structural damping matrix coefficients are $c_{11} = 1$, $c_{12} = 0$, $c_{21} = 0$ and $c_{22} = 6{\cdot}273$. The numerical values of the dimensionless flow-added damping matrix coefficients are $d_{11} = 0{\cdot}30$, $d_{12} = -0{\cdot}06$, $d_{21} = 0{\cdot}40$ and $d_{22} = 0{\cdot}09$.

In the case of a bi-articulated beam (with the same length for the two parts), the matrix can be directly calculated from the classical dynamic theorems. In our experimental beam the ratio of the stiffness due to the articulations on the stiffness due to the weight is 0·4. Then, the first natural frequency is $\omega_1 = 0{\cdot}659(g/L/2)^{1/2}$ and the ratio of the second to the first natural frequency is $\beta_2 = 3{\cdot}619$. The numerical values of the dimensionless flow-added stiffness matrix coefficients are $a_{11} = 0{\cdot}637$, $a_{12} = -1{\cdot}837$, $a_{21} = 0{\cdot}788$ and $a_{22} = -1{\cdot}948$. The numerical values of the structural damping matrix coefficients are $c_{11} = 0{\cdot}366$, $c_{12} = -0{\cdot}099$, $c_{21} = -0{\cdot}099$ and $c_{22} = 16{\cdot}159$. The numerical values of the dimensionless flow-added damping matrix coefficients are $d_{11} = 1{\cdot}646$, $d_{12} = -0{\cdot}3573$, $d_{21} = 1{\cdot}811$ and $d_{22} = 0{\cdot}321$.